ACS APPLIED MATERIALS & INTERFACES
Research Article
www.acsami.org

Improved Growth Behavior of Atomic-Layer-Deposited High-*k* Dielectrics on Multilayer MoS_2 by Oxygen Plasma Pretreatment

Jaehyun Yang,[†] Sunkook Kim,[‡] Woong Choi,[§] Sang Han Park,[⊥] Youngkwon Jung,[‡] Mann-Ho Cho,[⊥] and Hyoungsub Kim*,[†]

[†]School of Advanced Materials Science and Engineering, Sungkyunkwan University, Suwon 440-746, Korea
[‡]College of Electronics and Information, Institute for Laser Engineering, Kyung Hee University, Yongin 446-701, Korea
[§]School of Advanced Materials Engineering, Kookmin University, Seoul 136-702, Korea
[⊥]Institute of Physics and Applied Physics, Yonsei University, Seoul 120-749, Korea

Supporting Information

ABSTRACT: We report on the effect of oxygen plasma treatment of two-dimensional multilayer MoS_2 crystals on the subsequent growth of Al_2O_3 and HfO_2 films, which were formed by atomic layer deposition (ALD) using trimethylaluminum and tetrakis-(ethylmethylamino)hafnium metal precursors, respectively, with water oxidant. Due to the formation of an ultrathin Mo-oxide layer on the MoS_2 surface, the surface coverage of Al_2O_3 and HfO_2 films was significantly improved compared to those on pristine MoS_2, even at a high ALD temperature. These results indicate that the surface modification of MoS_2 by oxygen plasma treatment can have a major impact on the subsequent deposition of high-*k* thin films, with important implications on their integration in thin film transistors.

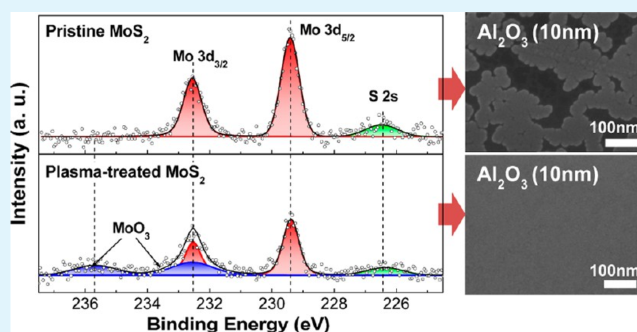

KEYWORDS: *MoS_2, oxygen plasma treatment, atomic layer deposition, Al_2O_3, HfO_2*

1. INTRODUCTION

There has been great interest in two-dimensional (2D) materials because of their intriguing electrical and optical properties, and because they are potentially applicable to future nanoscale and flexible electronic devices.[1,2] Although graphene is the most widely explored 2D material, the intrinsic absence of band gap limits its extended application to conventional switching devices, such as field-effect transistors (FETs).[2,3] Recently, as a 2D layer-structured transition metal dichalcogenide, molybdenum disulfide (MoS_2) has been emerging as a promising alternative candidate due to the existence of a relatively wide bandgap. A single layer has a direct bandgap of ~1.8 eV, whereas the bulk form has an indirect bandgap of ~1.2 eV.[4,5] With this fascinating advantage, several research groups have successfully demonstrated a field-effect mobility of 100−500 $cm^2/(V\ s)$, and a remarkable subthreshold swing as low as ~70 mV/dec using single or multilayer MoS_2 FETs, in which high-dielectric-constant (high-*k*) materials were formed by an atomic layer deposition (ALD) technique and adopted as a top or bottom gate dielectric layer.[6−8]

In these MoS_2 FET structures, engineering the high-*k* gate dielectric that covers the MoS_2 surface plays a critical role in the enhancement of carrier mobility in 2D-layered MoS_2. It was suggested that the dielectric engineering can strongly dampen the Coulombic scattering of charge carriers in the 2D-layered nanostructure through the dielectric constant mismatch effect between the nanoscale semiconducting material and the high-*k* dielectric.[9] For example, the field-effect mobility drastically drops down to 1−20 $cm^2/(V\ s)$ without an ALD high-*k* dielectric film on MoS_2.[10,11] Furthermore, as an additional benefit, the high-*k* layer on MoS_2 may reduce the hysteresis of FETs by preventing the moisture absorption from ambient air.[11]

However, because of the absence of dangling bonds or functional groups (e.g., hydroxyl groups) on the MoS_2 surface to react with ALD precursors, especially metal−organic (MO) precursors, Liu et al.[12] claimed that complete coverage of Al_2O_3 films could not be achieved at an elevated ALD temperature over 200 °C. They attributed it to the physically adsorbing nature of ALD precursors on MoS_2 with a much weaker binding energy than the chemical adsorption, and solved this problem by lowering the ALD temperature down to 200 °C.[8,12] Lowering the ALD temperature could be a facile way for acquiring a uniform and continuous high-*k* film on MoS_2. However, the electrical properties of the high-*k* film can be degraded with decreasing ALD temperature, because a large amount of carbon impurities released from MO precursors can remain in the high-*k* film.[13] In addition, structural defects such

Received: December 27, 2012
Accepted: May 20, 2013
Published: May 20, 2013

ACS Publications © 2013 American Chemical Society

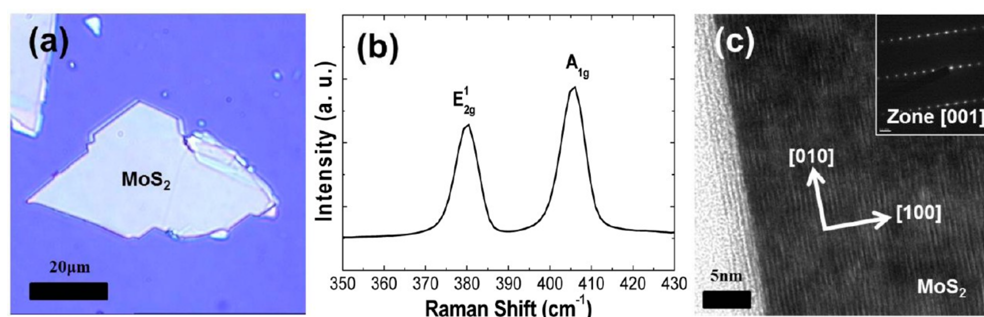

Figure 1. (a) Optical micrograph of the multilayer MoS_2 flake transferred on the SiO_2/Si substrate. (b) Raman spectra measured from the pristine MoS_2 flake. (c) Cross-sectional HRTEM image of the multilayer MoS_2 flake on the SiO_2/Si substrate. The inset in image c shows the SAED pattern obtained from the multilayer MoS_2 crystal.

as pinholes may not be completely removed, even at the optimal ALD temperature, which may vary depending on the precursor chemistry and hardware configuration.

As an alternative route to improving the film coverage at a wide range of ALD temperatures, we suggest an oxygen plasma pretreatment of the MoS_2 surface that supplies sufficient chemical adsorption sites. For this purpose, we compare the growth behavior of ALD-Al_2O_3 and HfO_2 films on multilayer MoS_2 crystals, with and without oxygen plasma pretreatment, and demonstrate much better deposition characteristics of the Al_2O_3 and HfO_2 films at various temperatures, even at a much higher temperature over 200 °C. Furthermore, we investigate the correlation between the oxygen plasma treatment and the chemical change of the MoS_2 surface.

2. EXPERIMENTAL SECTION

Multilayer MoS_2 flakes were isolated from a single crystal of 2H-MoS_2 (SPI, natural molybdenite) by a micromechanical exfoliation method using 3 M scotch tape, which is commonly used for the preparation of layer-structured 2D materials.[14] Then, the exfoliated MoS_2 flakes were transferred onto a p-type Si (100) wafer covered with a thermally grown SiO_2 film (300 nm). The transferred samples were soaked in acetone for 6 h to remove the possible adhesive residues,[12] followed by isopropanol cleaning for 30 s and N_2 blowing. To improve the adsorption of MO precursors on the MoS_2 surface during the subsequent ALD high-*k* growth process, some samples were further treated by oxygen plasma for different durations (10, 20, and 30 s) without intentional heating. The plasma was remotely generated by an inductively coupled plasma source operating at a power of 50 W. During the plasma treatment, oxygen gas was introduced at a flow rate of 25 sccm, and the process pressure was kept at 130 mTorr. The Al_2O_3 and HfO_2 deposition was carried out for various numbers of ALD cycles using trimethylaluminum (TMA)/water and tetrakis-(ethylmethylamino)hafnium (TEMAHf)/water precursor chemistries, respectively, in a custom-built thermal ALD system. One cycle of Al_2O_3 and HfO_2 deposition consists of a series of alternating precursor and purging gas injections for different durations in a reliable ALD regime, that involved TMA/N_2/H_2O/N_2 and TEMAHf/N_2/H_2O/N_2 injections for 0.5 s/10 s/1.5 s/15 and 1 s/10 s/1.5 s/15 s, respectively. The deposition rates of both ALD processes were separately monitored both on the thermally grown SiO_2 (300 nm)-covered and hydrogen fluoride (HF)-cleaned Si wafers, and measured by a spectroscopic ellipsometer (Nanoview SE-MG1000) (see Figure S1 in the Supporting Information).

The as-transferred and plasma-treated MoS_2 flakes were analyzed by Raman spectroscopy (WITEC ALPHA 300) using an Ar^+ laser with an excitation energy of 2.41 eV. The growth behavior of ALD-Al_2O_3 and HfO_2 films was examined both by scanning electron microscopy (SEM, JEOL JSM 7000F) and atomic force microscopy (AFM, SII SPA-300HV). The microstructural analysis of the samples was also performed by transmission electron microscopy (TEM, JEOL JEM 2100F) after fabricating cross-sectional TEM samples using a focused ion beam system (FIB, SII SMI 3050TB). Finally, X-ray photoelectron spectroscopy (XPS, ULVAC-PHI PHI5000) equipped with a monochromatic Al Kα (1486.7 eV) X-ray source was used to scrutinize the chemical effect of the oxygen plasma treatment on the MoS_2 surface.

3. RESULTS AND DISCUSSION

To confirm the successful transfer of the multilayer MoS_2 flakes on the receiving SiO_2/Si substrate, we undertook several evaluations. Figure 1a shows an optical micrograph of the transferred pristine multilayer MoS_2 flake, and its Raman spectra is shown in Figure 1b. We observed two typical Raman characteristic features of single-crystalline MoS_2, which corresponded well to those of the bulk 2H-MoS_2 crystal.[15] In-plane motion (E^1_{2g} mode) and out-of-plane vibration (A_{1g} mode) of Mo and S atoms near the Raman shifts of around 380 and 406 cm^{-1} were observed, respectively. The high-resolution TEM (HRTEM) image and the corresponding selected area electron diffraction (SAED) pattern shown in Figure 1c indicate the single-crystalline nature of the transferred multi-layer MoS_2 flake with an atomic arrangement of hexagonal symmetry.

At an ALD temperature of 250 °C, the growth behavior of both Al_2O_3 and HfO_2 films on the as-cleaned MoS_2 surface was compared with respect to the increasing number of deposition cycles, as shown in the plan-view SEM images of Figure 2. Because the hydrophobic Si surface has an early stage nucleation delay for the ALD process similar to the MoS_2 surface,[16,17] for convenience, the expected thicknesses of the

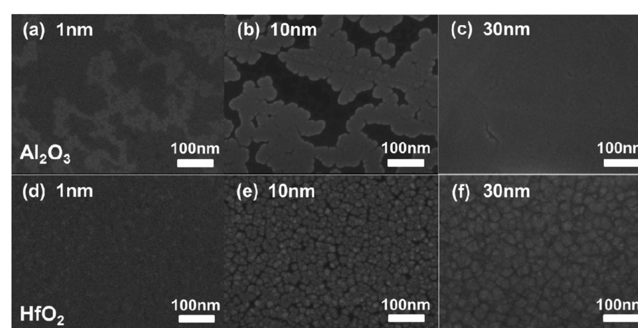

Figure 2. SEM images of the ALD-grown (a–c) Al_2O_3 and (d–f) HfO_2 films on the pristine MoS_2 flakes as a function of thickness. The ALD temperature was set at 250 °C and the number of ALD cycles was adjusted to form Al_2O_3 and HfO_2 films with thicknesses of (a, d) ~1 nm, (b, e) ~10 nm, and (c, f) ~30 nm on HF-last Si substrates.

Al_2O_3 and HfO_2 films grown on MoS_2 were expressed using the values, which correspond to the thicknesses of the films grown on the HF-last Si substrates. Based on the deposition rate on the HF-last Si surface (see Figure S1 in the Supporting Information), the ALD cycle numbers of 11, 110, and 330 were chosen for the formation of ∼1 nm, ∼10 nm, and ∼30 nm-thick Al_2O_3 films, respectively. For the HfO_2 deposition, the corresponding ALD cycle numbers were 14, 140, and 420. At the initial growth stage of ALD-Al_2O_3, corresponding to the formation of ∼1-nm-thick film on HF-last Si, we could observe dispersed and island-shaped film formation with a surface coverage of around 23%, as shown in Figure 2a. As the film thickens, unevenly located islands grow to be connected with each other like clusters, increasing the surface coverage to ∼77% and ∼97% for the ∼10 and ∼30-nm-thick films, respectively (Figure 2b, c). However, there remain many incomplete boundaries between the islands, even in the ∼30-nm-thick film. Recently, Liu et al.[12] observed a similar growth behavior of the ALD-Al_2O_3 film on MoS_2 with identical precursors. They reported strong temperature-dependent film coverage, and could obtain a continuous ∼10-nm-thick Al_2O_3 film by lowering the ALD temperature to 200 °C. Based on theoretical calculation, they claimed that the initial ALD-Al_2O_3 growth is predominated by the relatively weak physical adsorption of the ALD precursors rather than by the stronger chemical adsorption due to the absence of dangling bonds and functional groups on the pristine MoS_2 surface.[12] Similarly, we also observed a consistent increase in the film coverage with decreasing ALD temperature, but complete coverage of the ALD-Al_2O_3 film with an identical thickness to that in their experiment (∼10 nm) could not be achieved at 200 °C (see Figure S2 in the Supporting Information). Although the exact origin of this difference could not be verified at this stage, one possible explanation could be due to the difference in the ALD process parameters, such as pulsing/purging times and pressure, which have a strong impact on the adsorption and desorption probabilities of the ALD precursors on the MoS_2 surface.[12]

In contrast to the ALD-Al_2O_3 film, more uniform nucleation was observed in the ALD-HfO_2 film using TEMAHf and H_2O precursors, as shown in Figure 2d−f. Although the Al_2O_3 film exhibited sporadic nucleation and island-like growth behavior, the HfO_2 film grew with a higher density of uniformly distributed nanosized grains. Although an almost evenly covered HfO_2 film could be achieved even at a deposition temperature as high as 300 °C, many pinhole-like defects between nanosized grains due to the incomplete boundaries were still observed at a film thickness of ∼10 nm (see Figure S3 in the Supporting Information), which may act as a high-leakage current path.

As an attempt to provide a large number of reactive sites for the ALD precursors by chemically modifying the MoS_2 surface, the as-cleaned MoS_2 surface was treated by oxygen plasma. First, for the selection of optimal pretreatment time, the as-cleaned MoS_2 samples were plasma-treated for different times, and immediately loaded into the ALD system for the dielectric deposition. Figure 3 compares the SEM images of the plasma-treated MoS_2 samples followed by a deposition of ∼10-nm-thick Al_2O_3 and HfO_2 films at 250 °C. After the plasma pretreatment for 10 s, the Al_2O_3 film coverage was considerably improved compared to that on the MoS_2 without the plasma treatment (see Figure 2b); it increased from ∼77% to ∼93%. Nearly complete coverage without notable incomplete

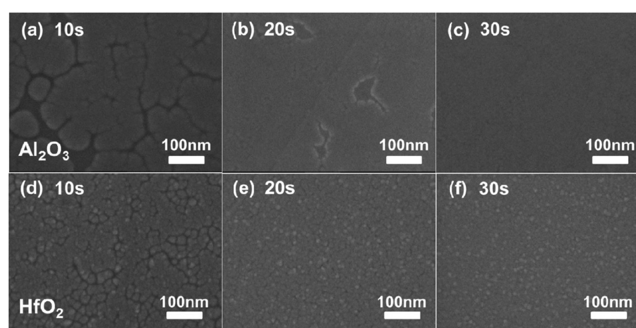

Figure 3. SEM images of the ALD-grown ∼10-nm-thick (a−c) Al_2O_3 and (d−f) HfO_2 films on the MoS_2 flakes pretreated with oxygen plasma for different times: (a, d) 10 s, (b, e) 20 s, and (c, f) 30 s. Both ALD processes were performed at 250 °C.

boundaries could be achieved after the 30 s treatment. A similar improvement of the film coverage with increasing plasma treatment time was also observed in the HfO_2 film case. For a confirmation, AFM surface scanning (1 μm × 1 μm) was performed on the Al_2O_3 and HfO_2 films deposited at 250 °C, and the extracted root-mean-square (RMS) surface roughness values are plotted as a function of the plasma treatment time in Figure 4. For both dielectrics, the plasma pretreatment reduced

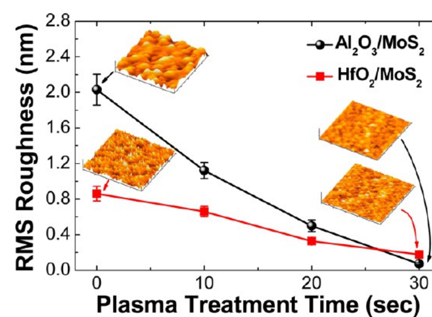

Figure 4. RMS surface roughness values of ∼10-nm-thick ALD-grown Al_2O_3 and HfO_2 films on MoS_2 as a function of the oxygen-plasma treatment time. Both ALD processes were performed at 250 °C. The AFM measurement was performed on a scanning area of 1 μm × 1 μm and the maximum height of the AFM images is 80 nm. The error bars in the graph represent one standard deviation from the average value obtained by five different measurements.

the RMS surface roughness. The monotonic decrease in the RMS surface roughness with increasing treatment time clearly indicates increased surface coverage with more uniform film formation, consistent with the observed SEM results. For the MoS_2 samples plasma-treated for less than 30 s, including the nontreated sample, the HfO_2 film showed a lower RMS surface roughness than the Al_2O_3 film, which is probably due to the more uniform and higher nucleation density of the HfO_2 film. After the 30 s plasma pretreatment, the lowest RMS surface roughnesses of ∼0.07 nm and ∼0.18 nm were achieved in the ∼10-nm-thick Al_2O_3 and HfO_2 films on MoS_2, respectively, which are similar to or less than the values measured from those films on Si (∼0.07 and ∼0.49 nm for ∼10-nm-thick Al_2O_3 and HfO_2 films on HF-last Si, respectively).

After choosing the plasma pretreatment time of 30 s, the growth behavior of the Al_2O_3 and HfO_2 films on the MoS_2 surface pretreated with oxygen plasma was examined again with a series of the high-k dielectric thicknesses at an ALD temperature of 250 °C. In comparison with the aforementioned

growth behavior on the pristine MoS_2 surface (see Figure 2), the growth characteristics of both high-*k* dielectrics were considerably improved, as shown in Figure 5. The large

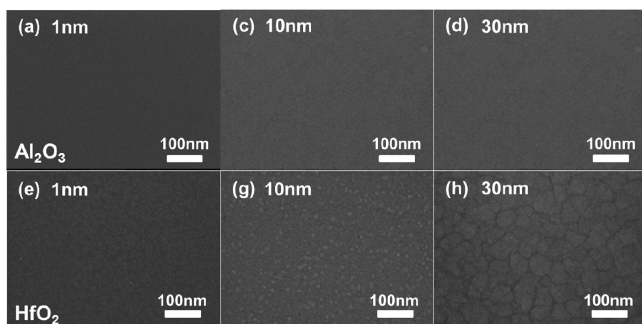

Figure 5. SEM images of the ALD-grown (a−c) Al_2O_3 and (d−f) HfO_2 films on the MoS_2 flakes pretreated with oxygen plasma for 30 s as a function of thickness. The ALD temperature was set at 250 °C and the number of ALD cycles was adjusted to form Al_2O_3 and HfO_2 films with thicknesses of (a, d) ∼1 nm, (b, e) ∼10 nm, and (c, f) ∼30 nm on HF-last Si substrates.

difference in surface coverage between the ALD-Al_2O_3 and HfO_2 films disappeared, and nearly complete coverage was obtained at the thickness of ∼10 nm for both dielectric films. Furthermore, even after increasing the temperature to 300 °C, similarly uniform film coverage could be achieved for both dielectrics (see Figure S4 in the Supporting Information). These presumably suggest that the MoS_2 surface was effectively modified to form more adsorption sites and to minimize the thermal desorption of MO precursors, thereby enabling uniform deposition of the high-*k* dielectric films.

Figure 6 exhibits cross-sectional TEM images of the Al_2O_3 and HfO_2 films grown on the multilayer MoS_2 crystal

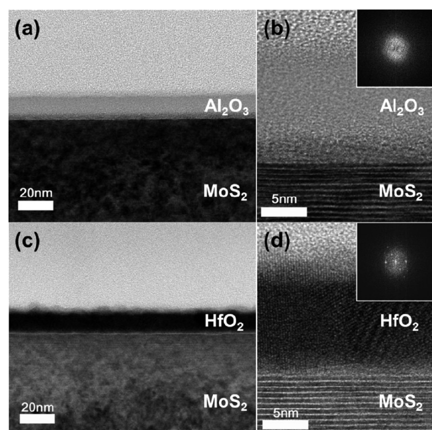

Figure 6. TEM images of ∼10-nm-thick ALD-grown (a, b) Al_2O_3 and (c, d) HfO_2 films on the MoS_2 flakes pretreated with oxygen plasma for 30 s. (b, d) High-resolution images of a and c. The insets of b and d show Fourier-transformed images obtained from the high-resolution TEM pictures of each dielectric film. Both ALD processes were performed at 250 °C.

pretreated with the oxygen plasma for 30 s. The cross-sectional images clearly reveal that uniform and continuous Al_2O_3 and HfO_2 films were successfully deposited on the multilayer MoS_2 after the oxygen plasma pretreatment. The as-grown Al_2O_3 and HfO_2 films have amorphous and polycrystalline states, respectively, as revealed from the Fourier-transformed images shown in the insets of Figures 6b and 6d. Although the number of deposition cycles for each process was set to be identical to form ∼10-nm-thick films on the HF-last Si substrates, the measured thickness was slightly increased to be around 13 nm. This may be attributed to the formation of an ultrathin new layer on the MoS_2 surface by the oxygen plasma treatment and also to the increase in the deposition rate by the effective conversion of the MoS_2 surface to a hydrophilic state. A similar increase in the ALD rates of the Al_2O_3 and HfO_2 films on the hydrophilic SiO_2 surface has been demonstrated, as shown in Figure S1 in the Supporting Information. A separate water contact angle measurement also revealed that the MoS_2 surfaces became more hydrophilic after the oxygen plasma treatment (see Figure S5 in the Supporting Information).

For more detailed analysis of the possible change of the MoS_2 surface by the oxygen plasma treatment, the surface regions of both the pristine and plasma-treated MoS_2 flakes were analyzed by XPS. Panels a and b in Figure 7 exhibit the

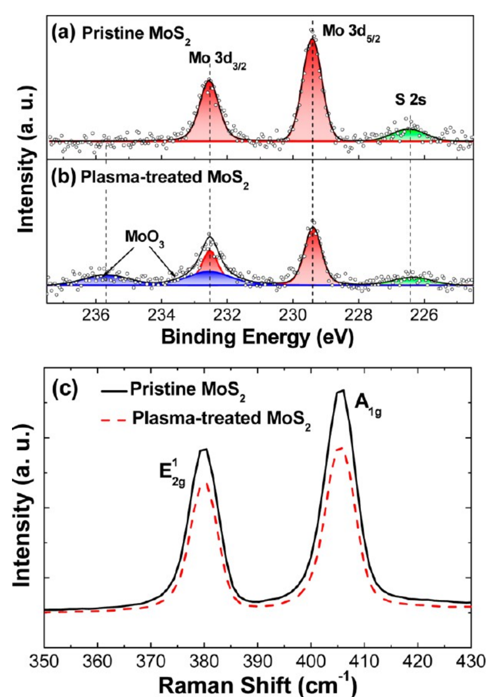

Figure 7. XPS spectra of Mo 3d and S 2s core levels measured from (a) pristine and (b) oxygen-plasma treated MoS_2 surface. The oxygen-plasma treatment was performed for 30 s. (c) Raman spectra measured on the identical spot of the MoS_2 flake before and after the oxygen plasma treatment. In Raman spectra, the maximum and minimum intensities were fixed for both samples.

binding energy region encompassing both the Mo 3d and S 2s core levels. For both samples, Mo^{4+} $3d_{3/2}$, Mo^{4+} $3d_{5/2}$, and S 2s peaks originating from Mo−S bonds in MoS_2 crystal were observed at binding energies of around 232.6, 229.4, and 226.4 eV, respectively.[18] After the oxygen plasma treatment, both the Mo^{4+} and S peak intensities were simultaneously decreased, which hints at possible partial conversion of MoS_2 into a different phase near the surface region by the oxygen plasma treatment. Because additional spin−orbit-coupled Mo 3d peaks appeared at a binding energy higher by ∼3.2 eV, which corresponds to the Mo^{6+} state in the MoO_3 phase,[18] it can be inferred that the newly formed phase on the surface region could be attributed to MoO_3. Because MoO_3 is known to be

hydrophilic,[19] it may provide many stronger chemical adsorption sites for the ALD MO precursors, minimizing their thermal desorption during the purging step. Also, a conformal coating of ALD-Al_2O_3 on crystalline MoO_3 nanoparticles was successfully demonstrated.[20] As a consequence, it can be concluded that more uniform and widespread ALD reaction would occur on the newly formed MoO_3 surface, which is sufficient to cover the whole MoS_2 surface, even at an early growth stage, as well as at a high deposition temperature.

Although the oxygen plasma treatment on the MoS_2 surface can help the ALD reaction occur more efficiently than on the pristine MoS_2 surface, there could be a concern on the possible induction of physical plasma damage, e.g., disordering of the MoS_2 lattice close to the surface, which may degrade the electrical properties of the multilayer MoS_2 crystal. To investigate this issue, we measured Raman spectra on the identical spot of the MoS_2 flake before and after the oxygen plasma treatment for 30 s. As shown in Figure 7c, the intensities of two characteristic Raman peaks were diminished after the plasma treatment, as compared to those before the treatment, probably because of the partial conversion of MoS_2 to the ultrathin Mo-oxide layer on the MoS_2 surface. However, no identifiable peak shift was observed, and similar full width at half-maximum values of these peaks were obtained after the plasma treatment: $\Delta\sim7$ and $\Delta\sim6$ cm^{-1} for E^1_{2g} and A_{1g} peaks, respectively. Although concrete confirmation warrants further study by fabricating top-gated FET devices and characterizing their electrical properties, it is tentatively believed that the plasma damage is minimal in this experiment, inducing no significant lattice disordering to such an extent as to change the electrical characteristics of the remaining MoS_2 crystal.

In addition to the Raman spectra measurement, the insulating property of the ALD dielectric films grown on the pristine and plasma-treated MoS_2 surfaces was further compared by fabricating simple two-terminal devices shown in Figure S6 in the Supporting Information. The ~50 nm-thick ALD-Al_2O_3 film deposited on the pristine MoS_2 surface exhibited a great increase in the leakage current, while that on the oxygen plasma-treated MoS_2 surface maintained a low leakage current level, comparable to the film deposited on Si (see Figure S7 in the Supporting Information). This indicates that the oxygen plasma pretreatment of the MoS_2 surface is beneficial in obtaining uniform coverage of the subsequently grown ALD-dielectric films and also has no negative impact on their insulating properties.

4. CONCLUSION

In summary, we have compared the ALD growth behavior of the Al_2O_3 and HfO_2 thin films on multilayer MoS_2 flakes, with and without oxygen plasma pretreatment. Without the plasma pretreatment, the TEMAHf/water-based ALD-HfO_2 film exhibited better surface coverage on the pristine MoS_2 surface than the TMA/water-based ALD-Al_2O_3 film at the same ALD temperature. However, as the plasma treatment time increased, the difference in the surface coverage became smaller, and after plasma treatment for 30 s, very thin layers (<10 nm) of Al_2O_3 and HfO_2 could be uniformly deposited, even at a higher deposition temperature over 200 °C. XPS analysis revealed that the improved growth behavior originated from the formation of an ultrathin Mo-oxide layer on top of the multilayer MoS_2 during the oxygen plasma treatment. Our results indicate that the optimized oxygen plasma treatment of MoS_2 surface can significantly improve the growth behavior of ALD high-k dielectrics on MoS_2, providing an important implication for integration in FET applications.

■ ASSOCIATED CONTENT

Supporting Information

ALD rates of Al_2O_3 and HfO_2 films as a function of temperature, SEM images showing thickness-dependent coverage of both dielectrics on pristine MoS_2 at various ALD temperatures, SEM images showing thickness-dependent coverage on 30 s plasma-treated MoS_2 at an ALD temperature of 300 °C, water contact angle measurement results, and detailed description on the two-terminal device fabrication and the corresponding leakage current characteristics. This material is available free of charge via the Internet at http://pubs.acs.org/.

■ AUTHOR INFORMATION

Corresponding Author

*E-mail: hsubkim@skku.edu.

Notes

The authors declare no competing financial interest.

■ ACKNOWLEDGMENTS

This work was supported by the Basic Science Research program (Grant 2012042548) and also by the World Class University program (Grant R32-2009-000-10124-0) through the National Research Foundation of Korea funded by the Ministry of Education, Science and Technology.

■ REFERENCES

(1) Wang, Q. H.; Kalantar-Zadeh, K.; Kis, A.; Coleman, J. N.; Strano, M. S. *Nat. Nanotechnol.* **2012**, *7*, 699−712.
(2) Geim, A. K. *Science* **2009**, *324*, 1530−1534.
(3) Schwierz, F. *Nat. Nanotechnol.* **2010**, *5*, 487−496.
(4) Mak, K. F.; Lee, C.; Hone, J.; Shan, J.; Heinz, T. F. *Phys. Rev. Lett.* **2010**, *105*, 136805.
(5) Kam, K. K.; Parkinson, B. A. *J. Phys. Chem.* **1982**, *289*, 463−467.
(6) Radisavljevic, B.; Radenovic, A.; Brivio, J.; Giacometti, V.; Kis, A. *Nat. Nanotechnol.* **2011**, *6*, 147−150.
(7) Kim, S. K.; Konar, A.; Hwang, W.-S.; Lee, J. H.; Lee, J.; Yang, J.; Jung, C.; Kim, H.; Yoo, J.-B.; Choi, J.-Y.; Jin, Y. W.; Lee, S. Y.; Jena, D.; Choi, W.; Kim, K. *Nat. Commun.* **2012**, 3 (1011), 1−7.
(8) Liu, H.; Ye, P. D. *IEEE Electron Device Lett.* **2011**, *33*, 546−548.
(9) Jena, D.; Kona, A. *Phys. Rev. Lett.* **2007**, *98*, 136805.
(10) Ghatak, S.; Pal, A. N.; Ghosh, A. *ACS Nano* **2011**, *5*, 7707−7712.
(11) Late, D. J.; Liu, B.; Matte, H. S. S. R.; Dravid, V. P.; Rao, C. N. R. *ACS Nano* **2012**, *6*, 5635−5641.
(12) Liu, H.; Xu, K.; Zhang, X.; Ye, P. D. *Appl. Phys. Lett.* **2012**, *100*, 152115.
(13) Swerts, J.; Peys, N.; Nyns, L.; Delabie, A.; Franquet, A.; Maes, J. W.; Elshocht, S, V.; Gendt, S. D. *J. Electrochem. Soc.* **2010**, *157*, G26−G31.
(14) Novoselov, K. S.; Jiang, D.; Schedin, F.; Booth, T. J.; Khotkevich, V. V.; Morozov, S. V.; Geim, A. K. *Proc. Natl. Acad. Sci. U.S.A.* **2005**, *102*, 10451−10453.
(15) Lee, C.; Yan, H.; Brus, L. E.; Heinz, T. F.; Hone, J.; Ryu, S. *ACS nano* **2010**, *4*, 2695−2700.
(16) Copel, M.; Gribelyuk, M.; Gusev, E. *Appl. Phys. Lett.* **2000**, *76*, 436−438.
(17) Hackley, J. C.; Gougousia, T.; Demaree, J. D. *J. Appl. Phys.* **2007**, *102*, 034101.
(18) Tai, S.-Y.; Liu, C.-J.; Chou, S.-W.; Chien, F. S.-S.; Lin, J.-Y.; Lin, T.-W. *J. Mater. Chem.* **2012**, *22*, 24753−24759.

(19) Gulbinski, W.; Pailharey, D.; Suszko, T.; Mathey, Y. *Surf. Sci.* **2001**, *475*, 149−158.
(20) Riley, L. A.; Cavanagh, A. S.; George, S. M.; Jung, Y. S.; Yan, Y.; Lee, S.-H.; Dillon, A. C. *ChemPhysChem* **2010**, *11*, 2124−2130.